

# A new test for evaluating crack sensitivity of materials during welding

Xiang Gao<sup>1</sup>, Wei Li<sup>1,2</sup>, Yi Fan<sup>2</sup>, Jiasheng Zou<sup>1</sup>, Keng Yan<sup>1</sup>, Jiaqing Tang<sup>1</sup>, Kun Liu<sup>1\*</sup>

<sup>1</sup>*School of Materials Science and Engineering, Jiangsu University of Science and Technology, Zhenjiang, 212100, P. R. China*

<sup>2</sup>*Jiangsu Key Laboratory for Premium Steel Materials, Nanjing Iron & Steel Co., Ltd., Nanjing 210035, P. R. China*

Received 1 March 2023, received in revised form 17 April 2023, accepted 21 April 2023

## Abstract

A new test was developed to evaluate the cracking sensitivity of thick plates based on the strong constraint conditions during the welding process. A typical application of the new test on assessing the cracking sensitivity of Q345R container steel was also investigated. The surface crack rate ( $\delta$ ) and the cross-section crack rate ( $\zeta$ ) both increased when setting the gap narrower. Crack rate and crack length both increased with increasing restraint stress. Under the critical constraint stress, the experimental results show that the welding heat input has no significant effect on crack sensitivity. With increasing carbon equivalent, the crack length and crack rate both increased. The aggregation of S and P was found near the crack, and the oxygen content was high. The fracture showed the characteristics of dendrites and microcrack, which was approved as a solidification crack.

**Key words:** rib plate restraint crack sensitivity test, numerical simulation, residual stress, critical constraint stress, crack sensitivity, solidification cracking

## 1. Introduction

At present, the commonly used welding cold crack tests mainly include the Y-shaped groove butt crack test, the cold crack test method for pin welding, the butt joint rigid restraint welding crack test method, the tensile restraint crack test (TRC), etc. The welding hot crack test mainly includes the adjustable restraint crack test and the pressure plate docking (FISCO) welding crack test. The conventional crack sensitivity test mainly has two limitations: one is that the test method is not closely related to the field welding, and the test constraint stress state has difficulty reflecting the actual welding situation; second, the constraint stress of some methods is less than the existing welding site, and it is difficult to predict the crack sensitivity of the welding site. Because of the above problems, according to the actual situation of field construction, a new test method for welding crack sensitivity is proposed: the method of rib plate restraint crack sensitivity. The sensitivity of the rib plate restraint method to the crack

is explored by means of numerical calculations and tests.

In the last decade, we have made great progress in understanding residual stresses and deformations in welded structures. In the context of pressure vessel and pipeline applications, Dong et al. [1] reviewed the latest advances in welding residual stress modeling procedures. Garza et al. [2] measured residual stresses using the deep hole drilling method, and the results were compared with those from finite element analysis with good agreement. Deng et al. [3, 4] used the three-dimensional thermal elastic-plastic deformation finite element method (FEM) to simulate the welding deformation of butt-welded joints of low-carbon steel. The welding temperature field, plastic strain distribution, and welding residual stress characteristics of the welded sheet were numerically analyzed. By comparing the simulation results with the measured results, it is found that the finite element prediction results of thermal elastic-plastic large deformation are in good agreement with the experimental values. Boellinghaus et al. [5, 8] explored the effects on a wide range of

\*Corresponding author: e-mail address: [liu\\_kun@163.com](mailto:liu_kun@163.com)

Table 1. Chemical constituents of Q345R and E711 (mass fraction, %)

Materials	C	Mn	P	S	Si	Al	Nb	Ti	Fe
Q345R	0.1	1.5	0.013	0.003	0.25	0.025	0.032	0.36	97.717
E711	0.059	1.41	0.016	0.008	0.41	–	–	–	98.097

parameters to give the reader a comprehensive understanding of what to consider when preparing for a weldability test. The effect of volume change caused by austenite-martensite transformation on final residual stress and welding deformation was treated. The final residual stress and welding deformation of low-carbon steel were not affected by HAZ solid phase transformation [6, 7].

Currently, the research on welding numerical simulation at home and abroad mainly focuses on the numerical simulation of thin plate welding, T-joints, thin small steel pipes, or the numerical simulation of welding for some new materials [9–11]. In the process of pressure vessel production, Q345R, as a widely used pressure vessel steel, is a kind of low alloy structural steel. Compared with ordinary carbon structural steel, it has high strength, good corrosion resistance, is lightweight, and has low-temperature performance. However, during the welding process, cracks sometimes occur under the strong constraint conditions of large and thick plates. Especially in the first welding process, cracks are more likely to initiate due to the enormous constraint stress.

Welding crack is one of the defects that have the greatest impact on the quality and performance of joints in equipment welding manufacturing. It not only reduces the strength of the weld but also is more likely to form a sharp notch at the end of the crack, causing serious stress concentration, resulting in failure of the welded structure and production safety accidents. Therefore, in the welding process, it is necessary to avoid the occurrence of welding cracks; especially in the welding and manufacturing of pressure vessels, the requirements for cracks are more stringent. A reliable and accurate evaluation method of welding crack sensitivity is a strong guarantee for joint quality.

## 2. Test materials and methods

### 2.1. Test materials

Q345R container steel was selected for the rib plate restraint test. Test plate parameters were ( $620 \times 268 \times 20 \text{ mm}^3$ ) with a V-shaped groove, a single groove angle of  $25^\circ$ , and a blunt root edge of 1 mm. The welding wire was an E711  $\phi 1.2 \text{ mm}$  flux-cored wire, and the material composition is shown in Table 1.

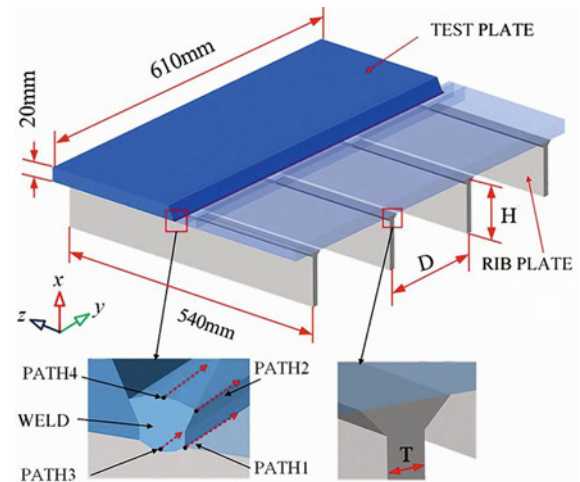


Fig. 1. Diagram of the rib restraint method.

### 2.2. Test method

Welding is a process of local rapid heating and subsequent rapid cooling. With the movement of the heat source, the temperature of the whole weldment changes sharply with time and space. The distribution of the welding temperature field is very uneven, and considerable welding stress and deformation will generate during welding. Before the test, a three-dimensional thermal elastic-plastic finite element model was established. The birth and death element method was used to simulate the weld filling and welding heat input process, and the dynamic stress and deformation during the whole welding process were realized. The welding temperature field and stress field of the rib plate were obtained, and the welding residual stress distribution of the rib plate was analyzed [3]. Through the calculation: find the significant constraint stress that is convenient to test, establish the model shown in Fig. 1, meshing grid, and calculate the simulated stress. The main factors affecting the restraint are the number of ribs ( $X$ ), the distance between ribs ( $D$ ), the height of ribs ( $H$ ), and the thickness of ribs ( $T$ ).

Based on the results of numerical calculations, large constraint stresses are selected to explore the test parameters and the effect of root clearance on crack sensitivity. Firstly, if cracks occur, the feasibility of the restraint crack sensitivity experiment of the rib plate is determined. Secondly, under strong restraint conditions, the test parameters and the root gap have

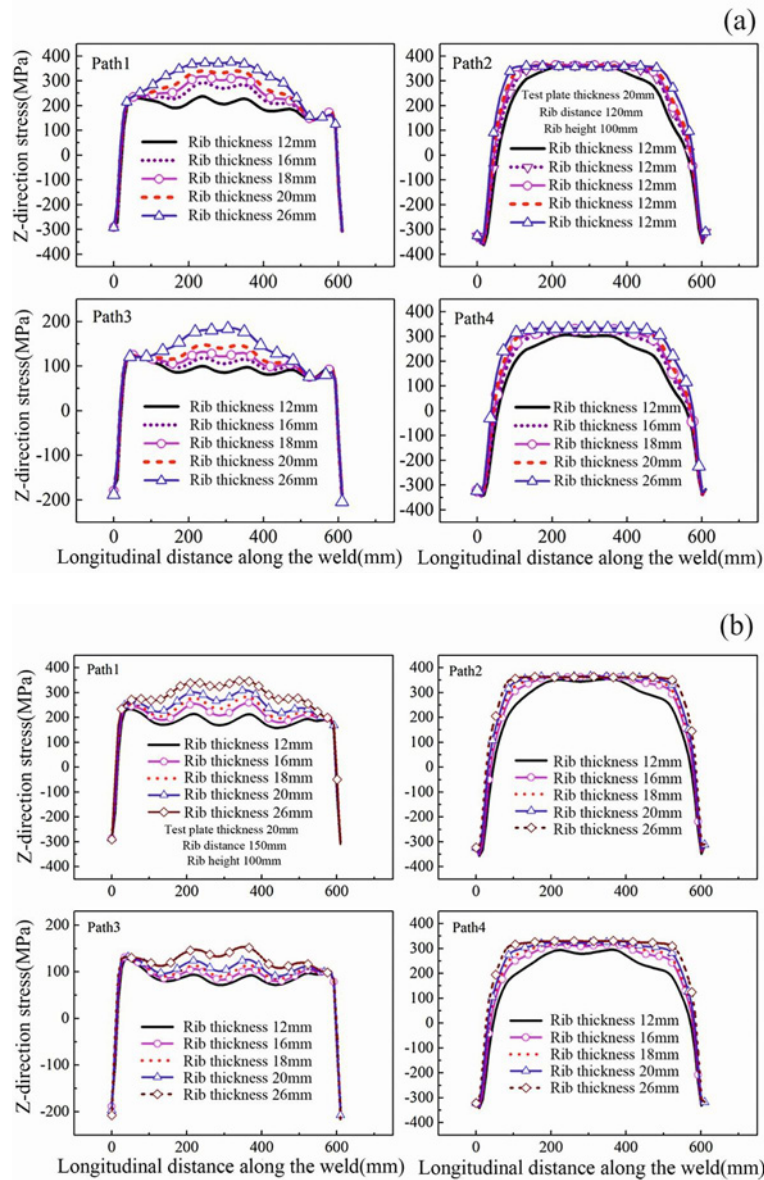


Fig. 2. Simulation of residual stress with different rib thicknesses: (a)  $D = 120$  mm,  $H = 100$  mm, and (b)  $D = 150$  mm,  $H = 100$  mm.

a significant impact on the crack sensitivity. In order to ensure that subsequent experiments reduce errors, it is necessary to determine the experimental plan. Based on the simulation law, find the critical value of the constraint stress. In the state of critical restraint stress, the influence of different factors on crack sensitivity can be more intuitively expressed, and the influence of different factors on crack sensitivity can be explored.

### 3. Test results and discussion

#### 3.1. Simulation result analysis

Firstly, the influence of rib thickness on con-

straint stress is investigated by numerical calculation. As shown in Fig. 2a, different rib thickness models are used to calculate the welding residual stress. For Path 1/Path 3, because close to the rib, the greater the thickness of the rib, the greater the  $Z$  residual stress. When the thickness of the rib exceeds 20 mm, the distribution of residual stress in Path 2/Path 4  $Z$ -direction is consistent. When the thickness of the test plate is 20 mm, Fig. 2b shows the distribution of the welding transverse residual stress on the four paths. For Path 1/Path 3, with the increase in the thickness of the rib, the  $Z$ -direction residual stress also increases. Therefore, from the simulation results in Figs. 2a,b, when the thickness of the rib exceeds 20 mm, the increase in restraint stress is not apparent; the rib

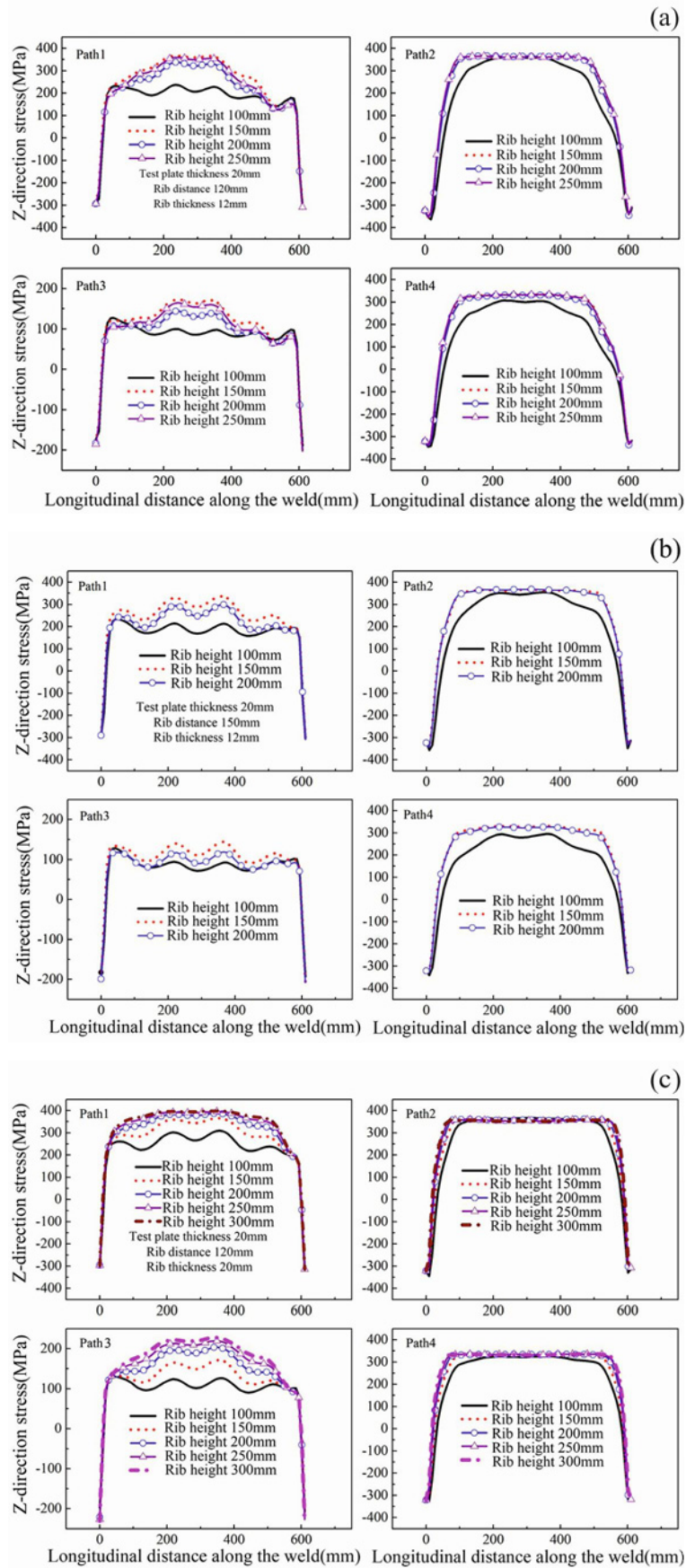


Fig. 3. Residual stress simulation diagram of different rib heights: (a)  $D = 120$  mm,  $T = 12$  mm, (b)  $D = 150$  mm,  $T = 12$  mm, and (c)  $D = 150$  mm,  $T = 20$  mm.

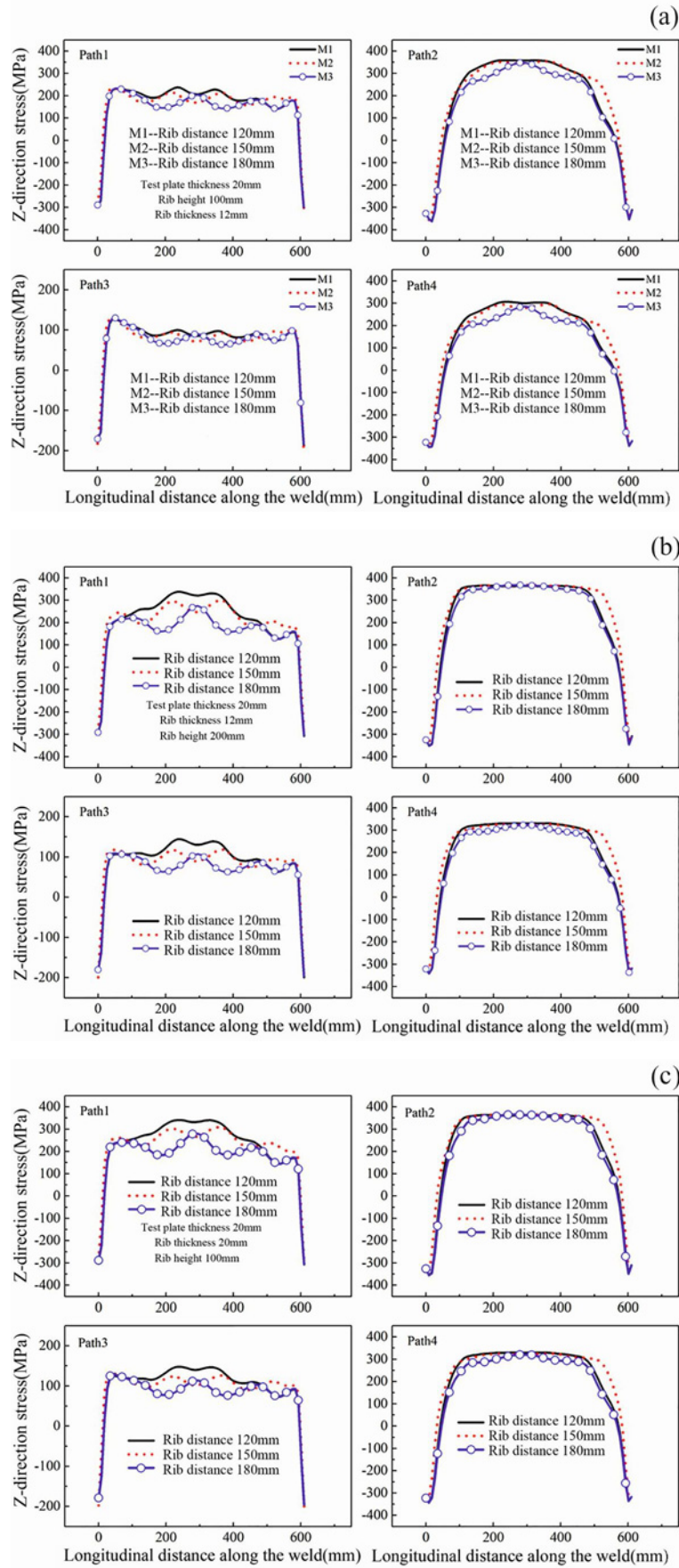


Fig. 4a–c. Simulation diagram of residual stress with different rib distance: (a)  $H = 100$  mm,  $T = 12$  mm, (b)  $H = 150$  mm,  $T = 12$  mm, (c)  $H = 200$  mm,  $T = 12$  mm.

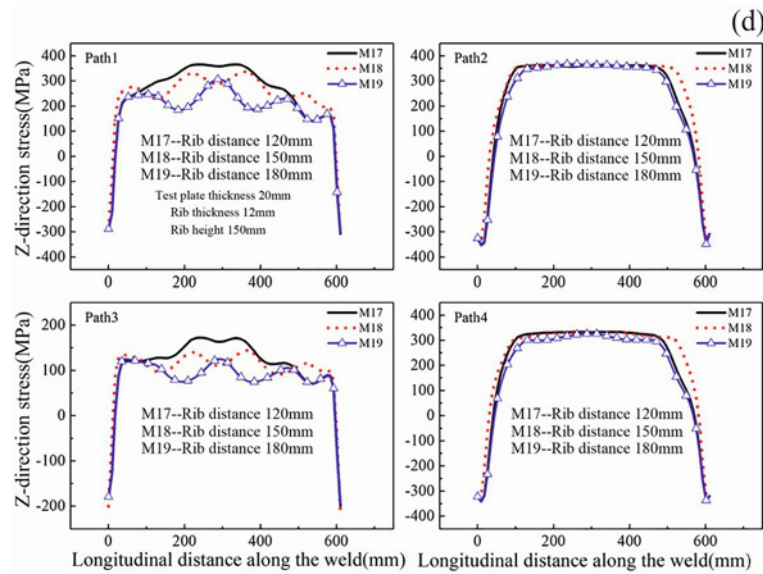


Fig. 4d. Simulation diagram of residual stress with different rib distance: (d)  $H = 100$  mm,  $T = 20$  mm.

Table 2. Specification and quantity of rib plate

Rib number $X$	Rib distance $D$ (mm)	Rib thickness $T$ (mm)	Rib height $H$ (mm)
5	120	20	150

with a thickness of 20 mm is selected as the test rib.

Secondly, the influence of rib height on restraint stress is investigated by numerical calculation. As shown in Fig. 3a, different rib height models are used to calculate the welding residual stress. When the rib height is 150 mm, for Path 1/Path 3, the restraint stress is the largest. When the rib height exceeds 150 mm, the Path 2/Path 4  $Z$ -direction residual stress curves almost coincide. In Fig. 3b, it can also be seen that for Path 1/Path 3, the peak value of the restraint stress is with the height of the ribs 150 mm, and for Path 2/Path 4, when the height of the test plate exceeds 150 mm, the distribution of the  $Z$ -direction residual stress is consistent.

Figure 3c shows that for Path 3 when the height of the ribs is increased from 150 to 300 mm, the peak value of the restraint stress increases by 40 % because it is close to the ribs. For Path 2/Path 4, when the test plate height exceeds 150 mm, the distribution of residual stress in the  $Z$  direction is basically the same. Therefore, from the simulation results in Fig. 3, combined with the actual situation of the test, the rib plate with a height of 150 mm is selected as the test rib plate.

Finally, the influence of rib distance on restraint stress is investigated by numerical calculation. First, as shown in Fig. 4a, the distribution of residual stress in the  $Z$  direction of the four paths is basically the

same, and the smaller the distance between the ribs is, the greater the constraint stress. Figure 4b shows Path 1/Path 3 is close to the rib plate, and the maximum stress appears at the position of the rib plate. With the decrease in the distance between the ribs, the  $Z$ -direction residual stress increases. The residual stress distribution of Path 2/Path 4 is basically the same. From the simulation results of Figs. 4c,d, the law is similar to Figs. 4a,b, so through the simulation analysis, combined with the actual situation, the rib distance of 120 mm is suitable as the test parameter.

Based on the stress simulation diagram of different rib plates, it can be seen that of the four paths, Path 3 has the most negligible constraint stress. The constraint stress is mostly between 100–200 MPa, so the probability of cracking is the smallest. Path 1 is close to the rib plate, at the weld toe on the lower surface of the weld, and the constraint stress reaches 350–400 MPa. However, due to the slight deformation of the root during the welding process, the cracking tendency is small. Path 2/4, located on the upper surface of the weld, the restraint stress is between 350–400 MPa, reaching the yield strength of the material, and the crack is more likely to appear on the upper surface of the weld.

Through numerical calculation, five ribs were determined. The height of the ribs ( $H$ ) was 150 mm, the thickness of the ribs ( $T$ ) was 20 mm, and the distance between the ribs ( $D$ ) was 120 mm. The ribs

Table 3. Welding parameters of the rib restraint method

Test number	Welding material	Current type and polarity	Welding current (A)	Arc voltage (V)	Welding speed (cm min <sup>-1</sup> )	Gas flow (L min <sup>-1</sup> )	Heat input (kJ cm <sup>-1</sup> )
1	E711	DCEP	220–240	30–32	15.0	15–25	18.22–21.20
2	E711	DCEP	220–240	37–38	15.9	15–25	21.19–23.75

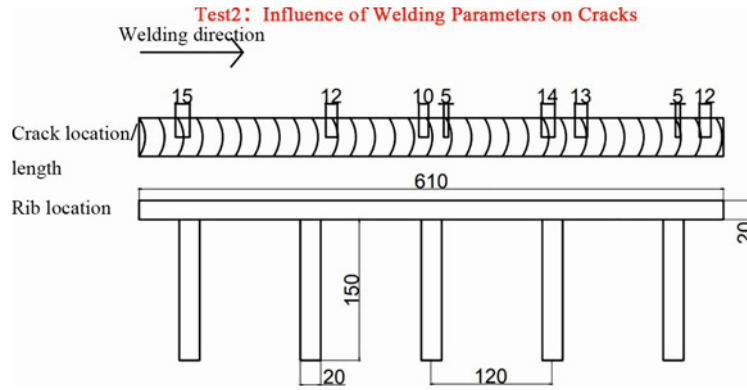


Fig. 5. Schematic diagram of test 2.

were welded to the test plate with a center distance of 120 mm. To reduce the deformation of the test plate, the method of interval and segmented welding was adopted. The size of the leg of the fillet weld ( $h$ ) was controlled at 6 mm. The welding of the ribs produces residual stress and affects the restraint stress state of the ribs. Therefore, to eliminate the influence of the residual stress generated by the welded ribs on the test results, the test plate was subjected to stress relief annealing after welding at 600–650 °C. The time was 210 (3 h + 30) min. Errors in root clearance were reduced, and unilateral groove control was held at 25°. Five ribs were used as much as possible to ensure that the rib height, rib thickness, and rib distance were consistent. The welding process was carried out by manual FCAW [13–15]; the welding gun did not oscillate, and the ceramic liner was placed close to the back. In order to avoid arc extinction (dry elongation 30–40 mm), the welding material was kept in contact with the molten pool, and the welding direction was from left to right. The rib plate specifications and quantities are shown in Table 2. Surface crack rate ( $\delta$ ) = crack length/total weld length. Post-weld sectioning, observation of cross-sectional cracking rates, observation of specimen sections, and counting of crack locations and crack lengths, section crack rate ( $\zeta$ ) = section crack length/weld thickness followed.

### 3.2. Effect of experimental parameters on test results

The test parameters have a significant influence

on weld forming [15], and it is of great significance to explore the influence of test parameters on crack sensitivity. The test design and parameters are shown in Table 3 to examine the effect of the change in test parameters on crack sensitivity.

In test 1, the weld was well formed, and no cracks were found on the front of the weld by the penetration test. The ceramic liner was removed, and the back penetration test was carried out. No cracks were found. The test parameters of test 1 were not sensitive to cracks.

In test 2, the weld was well formed. Cracks appeared on the front side of the test plate, cracks appeared in the weld center, and the crack direction was parallel to the weld. The back weld was well formed, observing the back and performing the penetration test on the back of the weld. The results are shown in Fig. 5, and there is no crack on the back of the weld. As shown in Fig. 5, it is found that welding cracks appear at the arc initiation, the middle section of the weld, and the arc extinguishing place of the weld. From Fig. 5, two 5–10 mm cracks and six 10–15 mm cracks can be obtained. The total crack length is 86 mm, and the surface crack rate ( $\delta$ ) is 14.1 %.

According to the test results, the arc voltage has a great influence on the crack sensitivity of the rib restraint method. Therefore, the welding test parameters are determined as shown in Table 4.

### 3.3. Effect of root clearance on test results

The root gap has a great influence on crack sensitivity, so it is necessary to study the effect of the root

Table 4. Welding parameters of the rib restraint method

Welding material	Current type and polarity	Welding current (A)	Arc voltage (V)	Welding speed ( $\text{cm min}^{-1}$ )	Gas flow ( $\text{L min}^{-1}$ )	Heat input ( $\text{kJ cm}^{-1}$ )
E711	DCEP	210–230	38–40	16–19	22	17.39–23.80

Table 5. Welding parameters of the wide and narrow gap tests

Test number	Welding material	Current type and polarity	Welding current (A)	Arc voltage (V)	Welding speed ( $\text{cm min}^{-1}$ )	Gas flow ( $\text{L min}^{-1}$ )	Heat input ( $\text{kJ cm}^{-1}$ )	Root gap (mm)
1	E711	DCEP	210–220	38–40	22.9	22	14.43–15.91	4.6–5.2
2	E711	DCEP	210–220	38–40	15.9	22	20.78–22.91	9.2–9.8

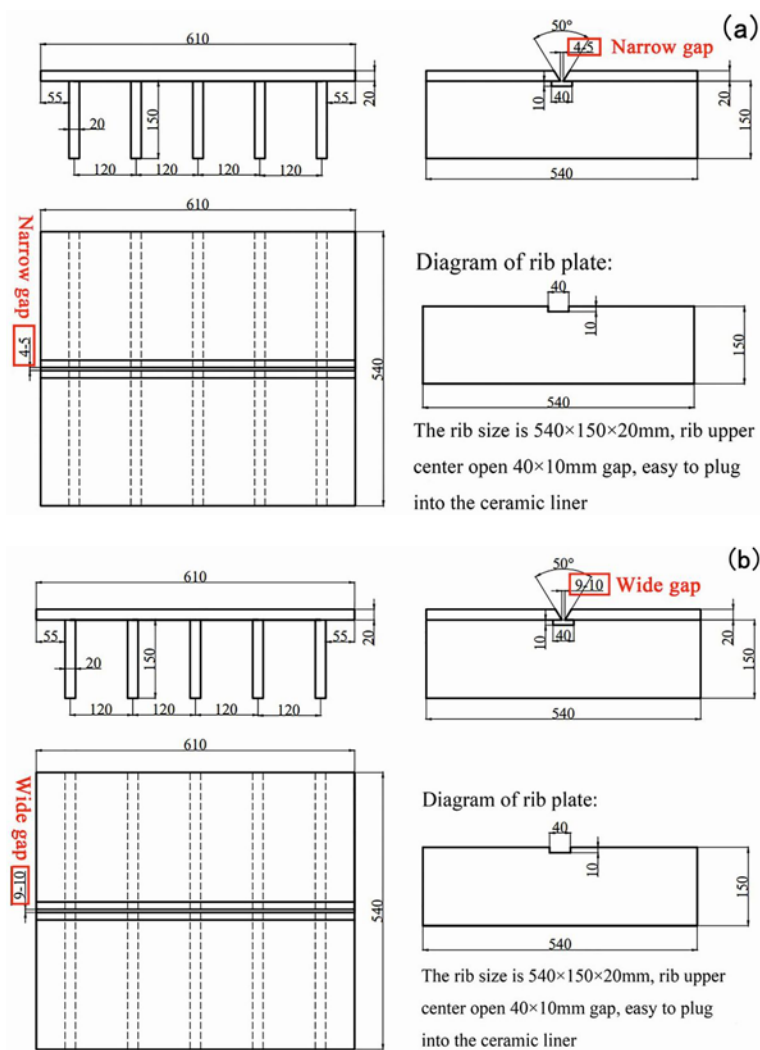


Fig. 6. Wide and narrow gap assembly diagram: (a) narrow gap and (b) wide gap.

gap on the crack rate [12]. According to the difference in root clearance, design test 1 is shown in Fig. 6a, and test 2 is shown in Fig. 6b. The narrow gap root clearance is 4.6–5.2 mm, the wide gap root clearance is 9.2–9.8 mm, and the welding parameters of test 1

and test 2 are shown in Table 5.

The narrow gap is shown in Fig. 7. The crack appears in the front center of the test plate, and the crack in Fig. 7c is parallel to the weld. Figure 7a shows the front penetration results of the narrow gap weld. It is

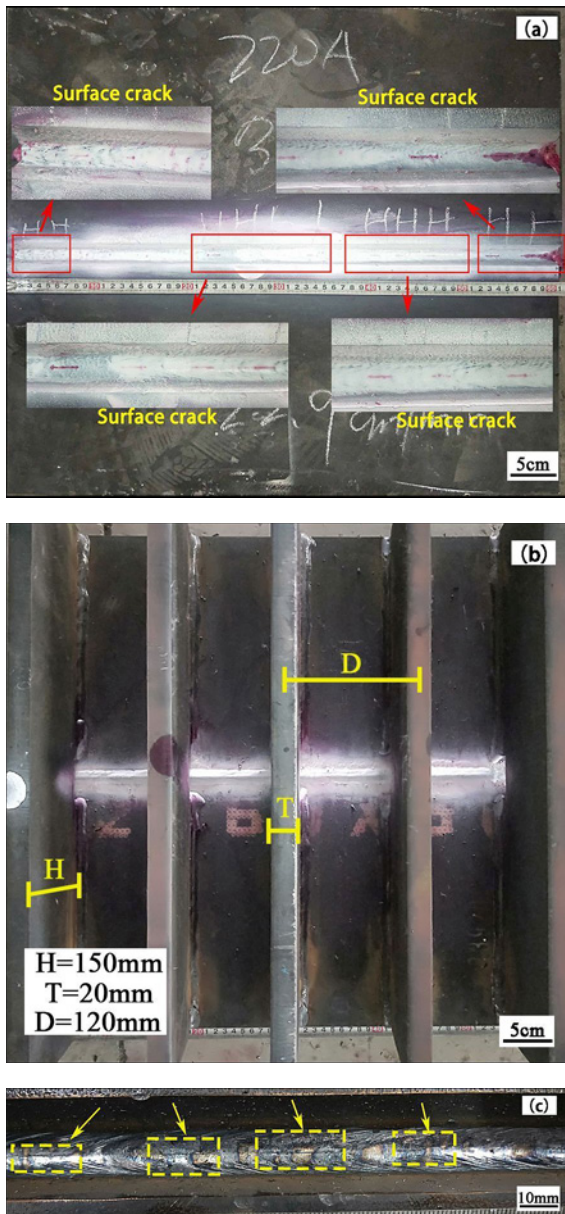


Fig. 7. Narrow gap test of the rib restraint method: (a) obverse side, (b) reverse side, and (c) surface crack.

found that welding cracks appear at the arc ignition, the middle section of the weld, and the arc extinguishing place of the weld. The back weld is well formed, observing the back and performing the penetration test on the back of the weld. The results are shown in Fig. 7b and there is no crack on the back of the weld.

During the test, due to the different gaps, to ensure the formation of the weld, the welding speed is considerably different, and the wide gap welding speed is significantly reduced. The wide gap test is shown in Fig. 8, with a crack parallel to the weld. Figure 8a shows the front penetration results of the narrow

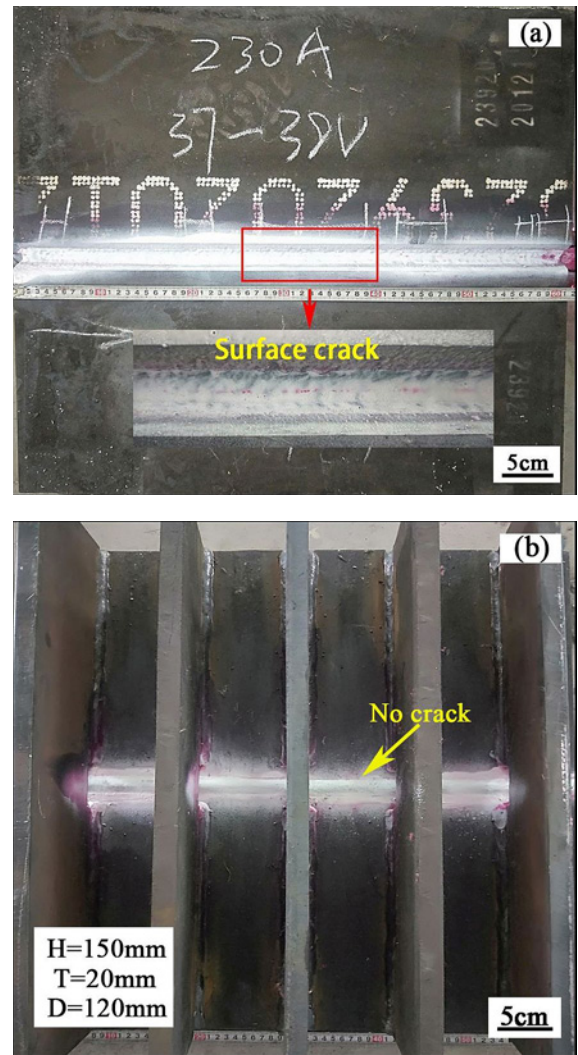


Fig. 8. Wide gap test of the rib restraint method: (a) obverse side and (b) reverse side.

gap weld, observing the back and performing the penetration test on the back of the weld. The results are shown in Fig. 8b, and there is no crack on the back of the weld.

As shown in Fig. 9, the wide and narrow gap rib plate restraint method crack position diagram, Fig. 9a shows five 5–10 mm cracks, five 10–15 mm cracks, and a 32 mm crack at the end. The total crack length is 128 mm, and the surface crack rate ( $\delta$ ) is 20.9%. The location of the crack is closely related to the location of the rib. Because of the maximum restraint stress at the rib, the location of the crack mostly appears near the rib. Figure 9b shows two 5–10 mm cracks and six 10–15 mm cracks. The total crack length is 86 mm, and the surface crack rate ( $\delta$ ) is 14.1%. The root gap significantly affects the crack sensitivity of the rib plate restraint crack test, and the surface crack rate ( $\delta$ ) of the narrow gap test is substantially higher than that of the wide gap test.

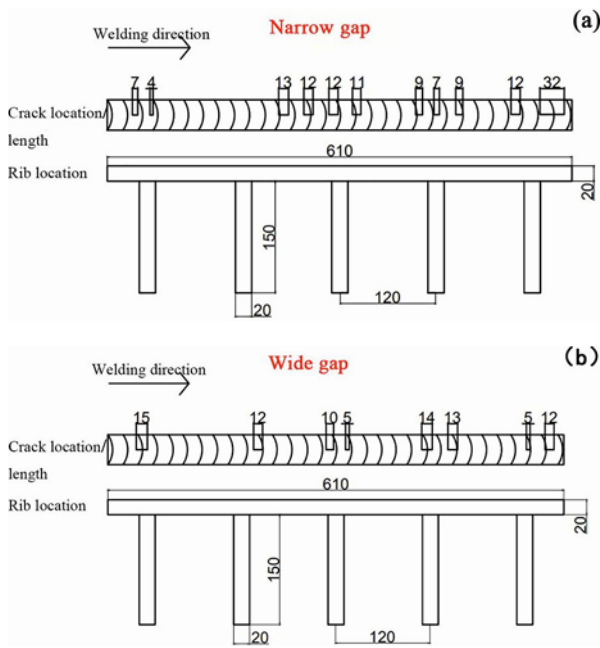


Fig. 9. Crack position diagram of the wide and narrow gap rib restraint methods: (a) narrow gap and (b) wide gap.

The metallographic structure of the narrow gap rib restraint crack is shown in Fig. 10a. As shown in Fig. 10c, the weld thickness is 7.8 mm, the crack length is 2.1 mm, and the section crack rate ( $\zeta$ ) reaches 27.1%. The metallographic structure of the crack of the wide gap rib restraint method is shown in Fig. 10b. As shown in Fig. 10d, the weld thickness is 6.9 mm, the crack length is 1.0 mm, and the section crack rate ( $\zeta$ ) is 14.5%. Weld cracks spread downwards from the upper surface. The most common is the longitudinal crack along the weld center. The section crack rate

( $\zeta$ ) of the narrow gap test is higher than that of the wide gap test. This is because the gap is small. During the welding process, the fusion ratio is relatively large, and the base material melts more, which results in the restraint stress of the rib plate being more reflected in the weld. As a new method for detecting crack sensitivity, the rib restraint method requires avoiding the influence of welding materials as much as possible and reflecting the sensitivity of the base metal to cracks as much as possible. Therefore, the fusion ratio is large, which can better meet the design requirements of the rib restraint method. In the rib restraint method, the narrow gap is selected as the test requirement, and the root gap should be kept at 4–5 mm.

### 3.4. Effect of constraint on test results

The rib plate restraint method simulates the restraint stress under actual production conditions. By adding rib plates to limit the deformation of the test plate, tensile stress is applied to the weld to achieve the purpose of detecting crack sensitivity. The restraint stress applied to the test plate by the rib restraint method is much higher than the restraint stress under the actual production conditions, and the conditions are more stringent. To investigate the effect of restraint stress on crack susceptibility, it is necessary to find critical restraint stress. According to the simulation results, the main factors affecting the restraint are the number of ribs ( $X$ ), the distance between ribs ( $D$ ), the height of the ribs ( $H$ ), and the thickness of the ribs ( $T$ ), as shown in Table 6, the following sets of tests were designed to find the critical restraint stress.

As shown in Fig. 11, five 20 mm rib plates, with a root gap of 2.6–3.1 mm, a total crack length of 90 mm, and a surface crack rate ( $\delta$ ) is 14.8%; two 20 mm rib

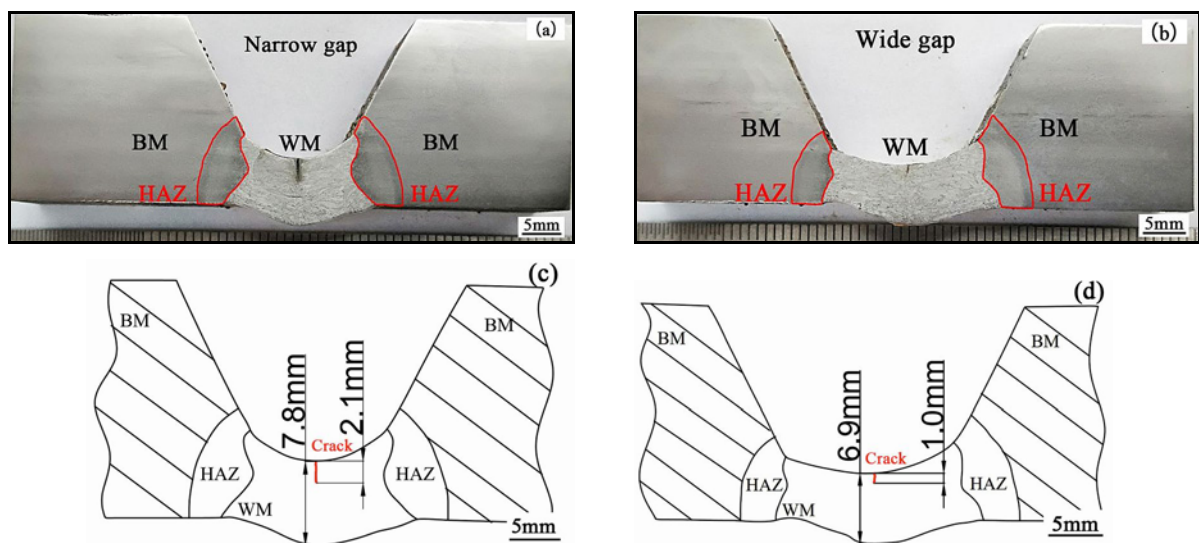


Fig. 10. Metallographic diagram of a normal section of wide-narrow gap rib restraint: (a), (c) narrow gap and (b), (d) wide gap.

Table 6. Welding parameters and root gap under different restraint stresses

Test number	Welding material	Current type and polarity	Welding current (A)	Arc voltage (V)	Welding speed (cm min <sup>-1</sup> )	Gas flow (L min <sup>-1</sup> )	Heat input (kJ cm <sup>-1</sup> )	Root gap (mm)
1	E711	DCEP	210–220	38–40	16.9	22	19.55–21.56	2.6–3.1
2	E711	DCEP	208–220	38–40	18.9	22	17.31–19.28	3.2–3.6
3	E711	DCEP	208–214	38–40	16.2	22	20.20–21.88	3.6–4.1
4	E711	DCEP	216–224	38–39	17.2	22	19.76–21.03	3.9–4.3

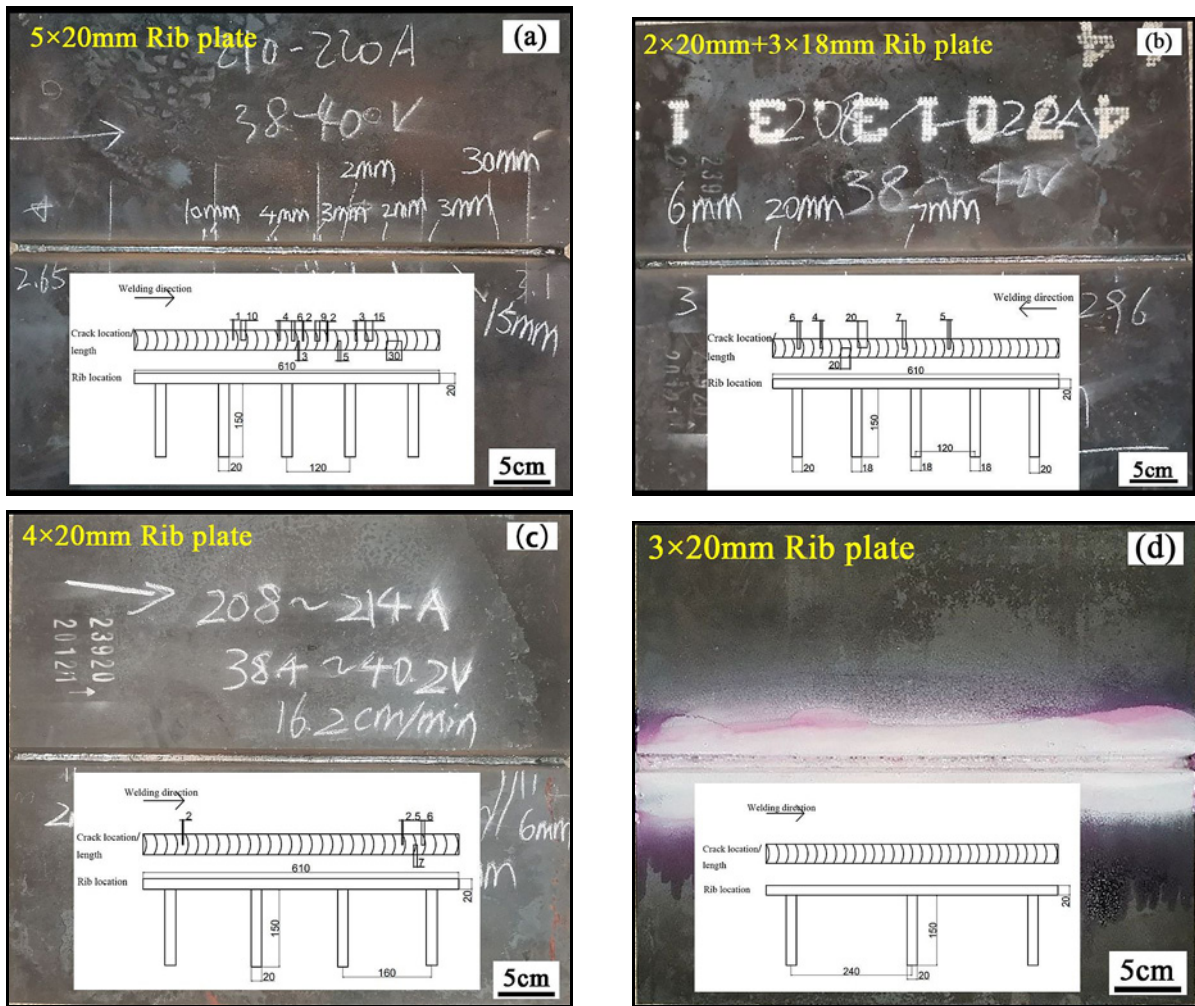


Fig. 11 Test results under different restraint stresses: (a) 5 × 20 mm, (b) 2 × 20 mm + 3 × 18 mm, (c) 4 × 20 mm, and (d) 3 × 20 mm.

plates and three 18 mm rib plates were used, with a root gap of 3.2–3.6 mm, a total crack length of 62 mm, and the surface crack rate ( $\delta$ ) is 10.0%; using four pieces of 20 mm rib plates with a gap of 3.6–4.1 mm, the total crack length is 22 mm, and the surface crack rate ( $\delta$ ) is 3.6%; using three pieces of 20 mm rib plates with a gap of 3.9–4.3 mm, the total crack length is 0 mm, and the crack rate is 0. The law of the effect of constraint on cracking can be obtained in Fig. 13. With the increase in constraint stress, the crack rate and the crack length increased.

The residual stresses were calculated by four different detention models [16, 17] (5 × 20 mm, 2 × 20 mm + 3 × 18 mm, 4 × 20 mm, 3 × 20 mm), and the results of the four paths were averaged, as presented in Eq. (1). The occurrence of cracks in the weld is not only related to a certain path but is generated under the influence of the comprehensive residual stress of the weld. Therefore, the results of the four paths are averaged to quantitatively express the influence of restraint on crack sensitivity, and the ex-

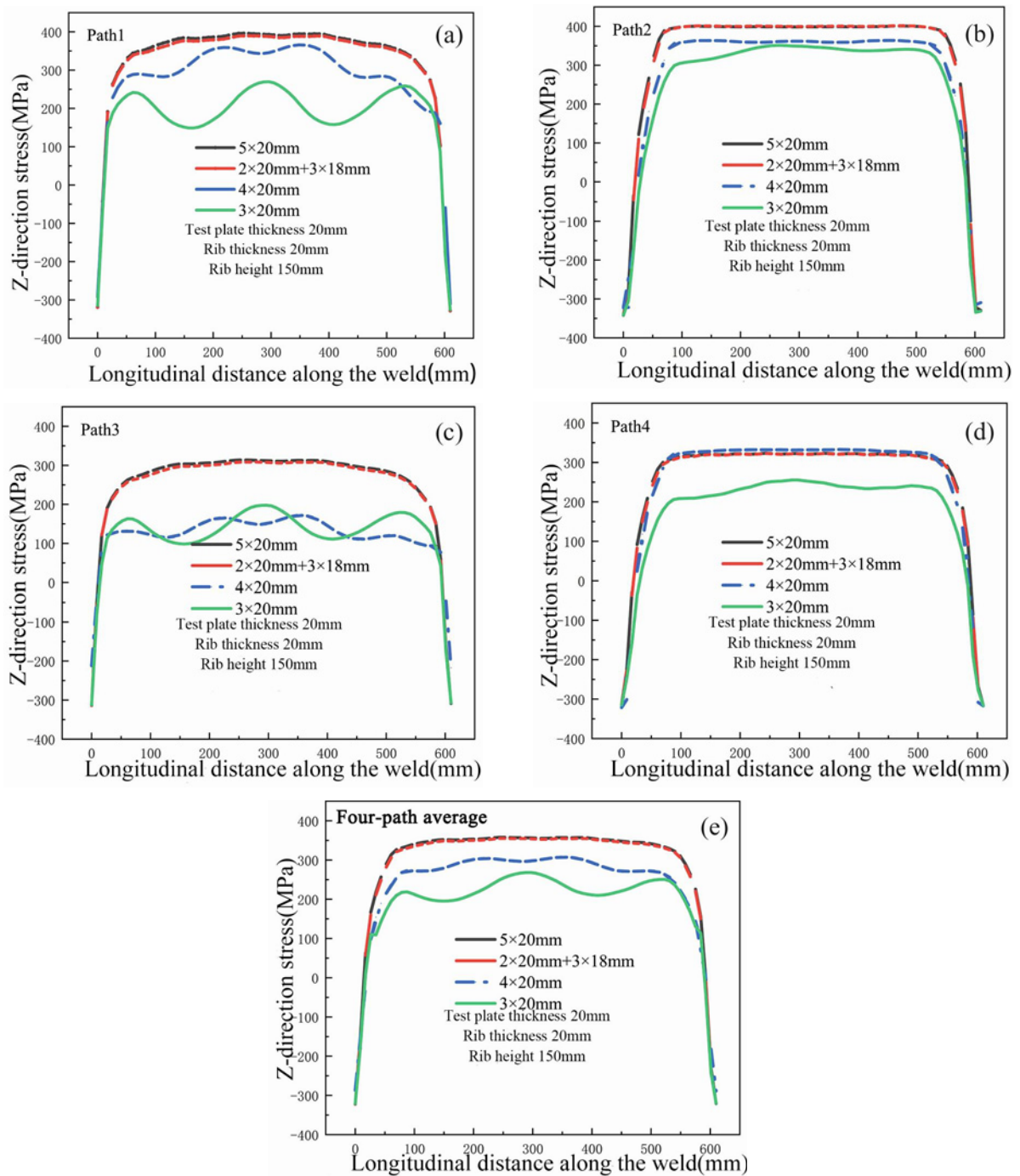


Fig. 12. Simulation diagram of residual stress: (a) path1, (b) path2, (c) path3, (d) path4, and (e) average.

perimental results are shown in Fig. 12.

$$\frac{\sum_{n=1}^4 \text{Path } n}{4} = \text{Average.} \quad (1)$$

From the stress simulation graph [16], it can be seen that the residual stress after welding increases significantly with the increase in the number of rib plates. And as the number of rib increases, especially when

the number of rib increases to 5, the fluctuation of the stress curve decreases significantly, and the residual stresses along the weld are distributed more uniformly.

The constrained state of the four 20 mm rib plates can be approximated as the critical constrained stress we are looking for. In the critical restraint stress, it is possible to explore on this basis: (i) The effect of heat input on crack sensitivity; (ii) The effect of base material composition (carbon equivalent) on crack sensitivity.

Table 7. Test results at different heat inputs

Test number	Welding material	Current type and polarity	Welding current (A)	Arc voltage (V)	Welding speed (cm min <sup>-1</sup> )	Gas flow (L min <sup>-1</sup> )	Heat input (kJ cm <sup>-1</sup> )	Crack length (mm)
1	E711	DCEP	166–175	32.9	12.2	15–25	18.53–19.54	28
2	E711	DCEP	279–284	38.6	16.6	15–25	26.86–27.34	30

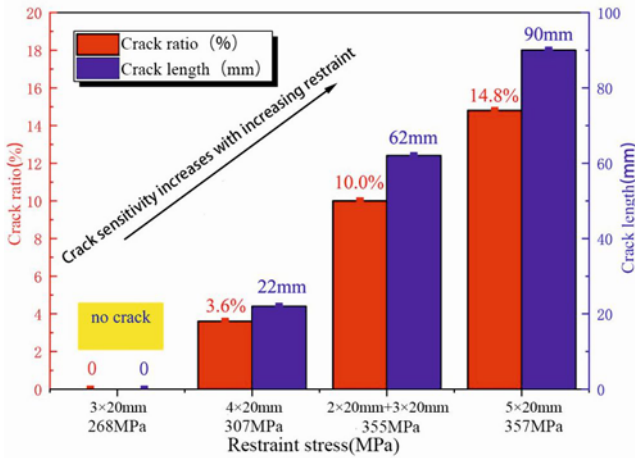


Fig. 13. Crack length and crack rate under different constraint stresses.

### 3.5. Effect of heat input and carbon equivalent on crack sensitivity

According to the test results as shown in Table 7, when the heat input is 18.53–19.54 kJ cm<sup>-1</sup>, the total crack length is 28 mm, and the surface crack rate is 4.5 %; when the heat input is 26.86–27.34 kJ cm<sup>-1</sup>, the total crack length is 30 mm, the surface crack rate is 4.9 %. According to the experimental results, it can be seen that with the increase in heat input, the crack length, as well as the increase in crack rate, are not significant; it can be considered that the experimental results of welding heat input are not significant.

Carbon equivalent experimental conditions are shown in Table 8. As shown in Fig. 14a,  $C_{eq} = 0.37$ , the total crack length is 4 mm, and the surface crack rate is 0.6 %; in Fig. 14b,  $C_{eq} = 0.41$ , the total crack length is 22 mm, and the surface crack rate is 3.6 %; in Fig. 14c,  $C_{eq} = 0.43$ , the total crack length is 31 mm, and the surface crack rate is 5.1 %. With the increase of carbon equivalent, the crack length as well as crack rate both increase.

The effects of heat input and carbon equivalent on the crack rate are shown in Fig. 15; it can be considered that the experimental results of welding heat input are not significant. The effect of carbon equivalent on crack sensitivity is more significant.

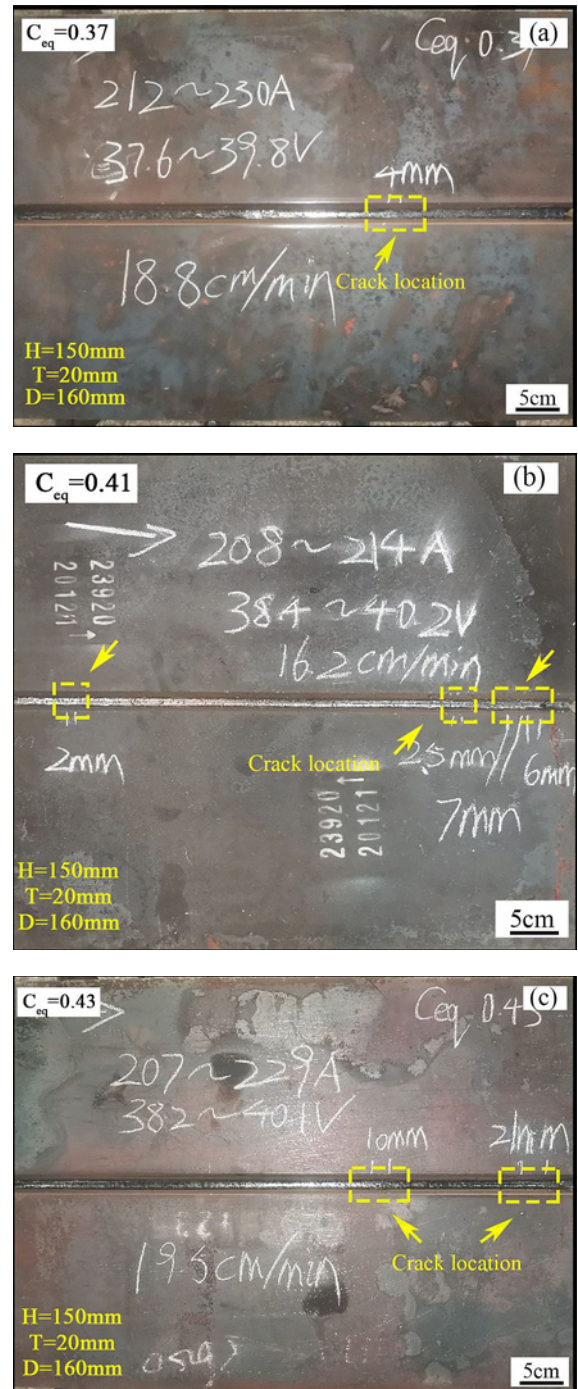


Fig. 14. Test results under different carbon equivalent: (a)  $C_{eq} = 0.37$ , (b)  $C_{eq} = 0.41$ , and (c)  $C_{eq} = 0.43$ .

Table 8. Test results at different carbon equivalent

Test number	Welding material	Current type and polarity	Welding current (A)	Arc voltage (V)	Welding speed (cm min <sup>-1</sup> )	Gas flow (L min <sup>-1</sup> )	Heat input (kJ cm <sup>-1</sup> )	Carbon equivalent $C_{eq}$
1	E711	DCEP	212–230	37.6–39.8	18.8	15–25	17.55–20.16	0.37
2	E711	DCEP	208–214	38–40	16.2	15–25	20.20–21.88	0.41
3	E711	DCEP	207–229	38.2–40.1	19.5	15–25	16.79–19.05	0.43

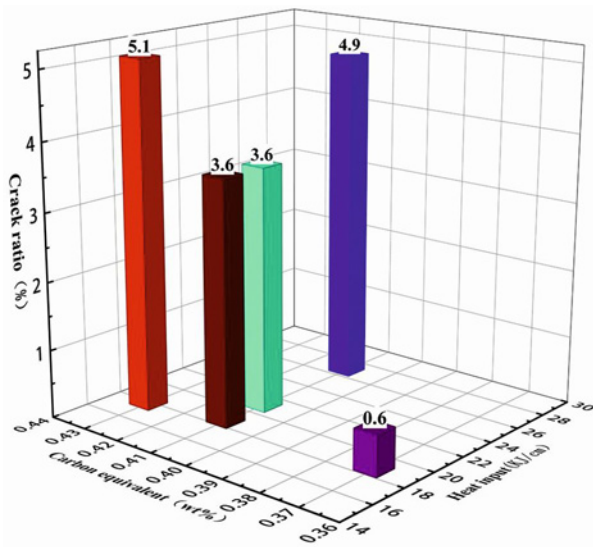


Fig. 15. Effect of heat input and carbon equivalent on crack rate.

### 3.6. Crack analysis

According to the appearance time and location of the crack, it is preliminarily judged to be a hot crack [14]. During the crystallization process of the weld, near the solid phase line, due to the solidification of the liquid metal, the metal shrinks, and the residual liquid metal is insufficient and cannot be filled in time. Under the action of stress, intergranular cracking occurs.

As shown in Fig. 16, the weld cracks along the center and is perpendicular to the growth direction of the weld columnar crystal. Both sides of the crack are uniform columnar crystals. The columnar crystal grows to the center of the weld, columnar crystal tips contact each other, and columnar crystal growth stops. In the late stage of weld metal crystallization, due to the low melting point of the eutectic, it is crowded out at the front end of the columnar crystal. The post-crystallized metal is a low-melting-point component, containing more impurities, and is enriched at the forefront of the columnar crystal or at the junction of adjacent columnar crystals. The formation of the so-called “liquid film” isolates the connection between the grains and makes the grain boundary a weak zone. The liquid film is the internal cause of crystal cracks, and tensile stress is the external cause of crystal cracks.

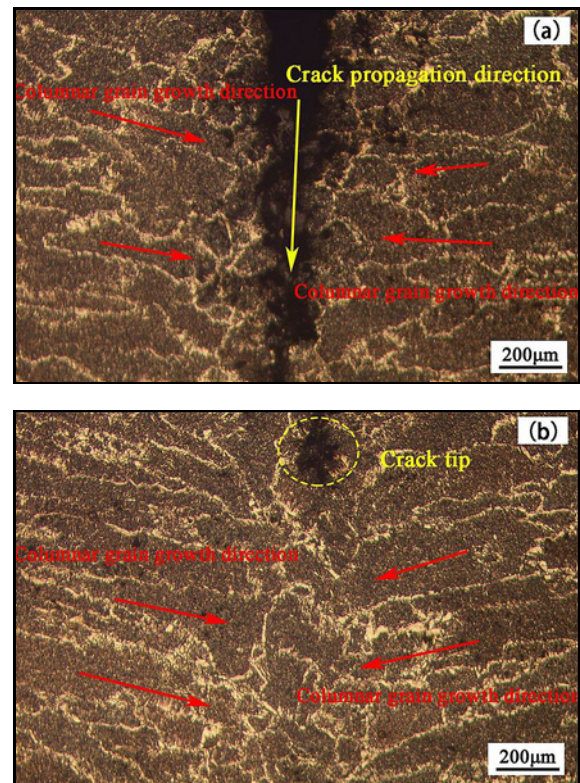


Fig. 16. Microstructure diagram of cracks: (a) crack and (b) crack tip.

Sulfur and phosphorus will increase the tendency of solidification cracks. They will expand the crystallization temperature range and increase the crack sensitivity. Sulfur and phosphorus are elements that are easily segregated in steel, and it easily forms a variety of low-melting eutectics at the grain boundaries, thus significantly increasing the crack tendency. As shown in Fig. 17, at the beginning of the crack, the aggregation of S and P was found near point A, and the oxygen content was higher. Near the crack propagation, two points C, D were found to have higher S and P content. Carbon is the main element affecting the crystallization crack in steel and can aggravate the harmful effects of sulfur and phosphorus. The columnar crystal intersects at the center of the weld, and the segregation degree of S and P elements is the highest. The melting point of the metal in these areas is the lowest, and the tendency to produce crystalline cracks is greater.

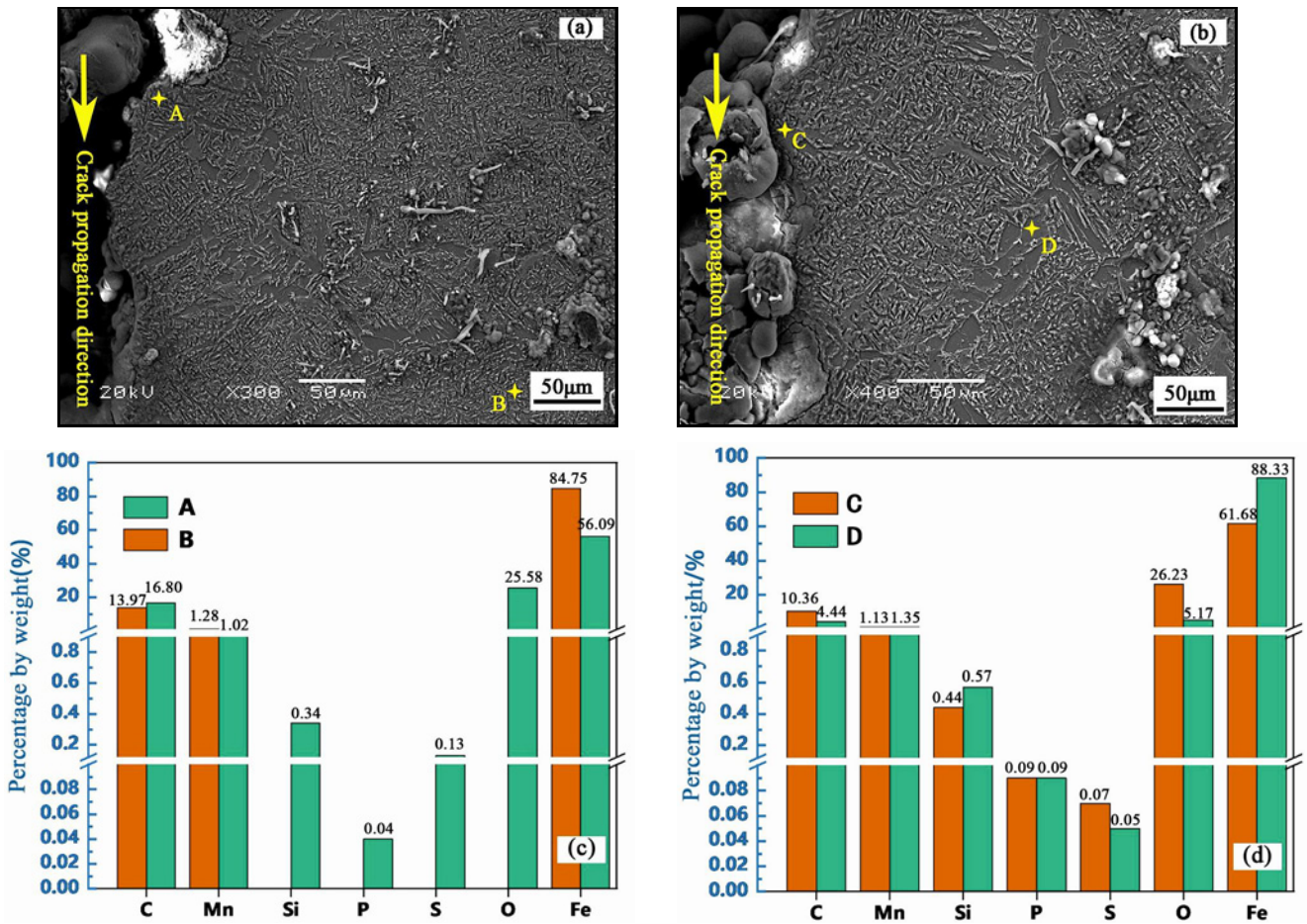


Fig. 17. Crack microstructure and EDS component scanning: (a) crack initiation and (b) crack propagation.

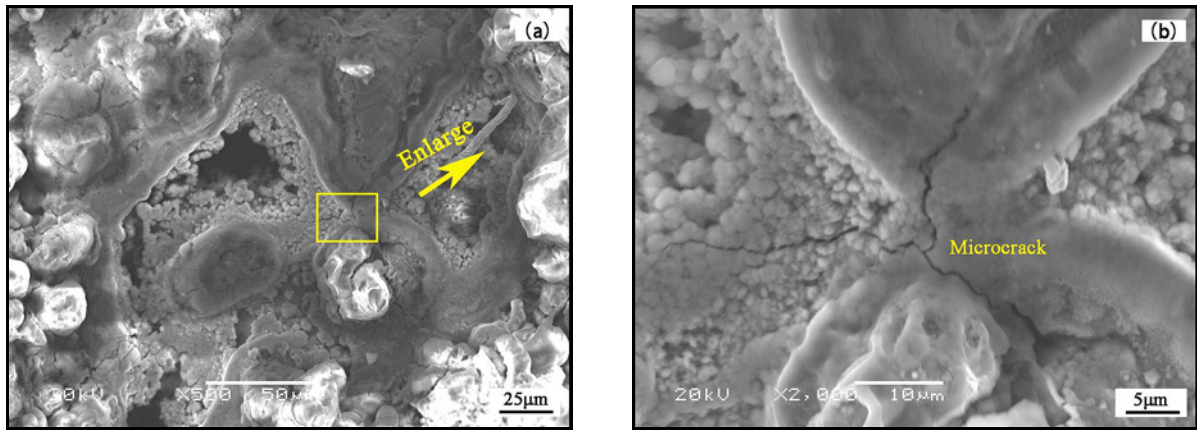


Fig. 18. Crack fracture morphology: (a) fracture surface and (b) amplification of fracture surface.

As shown in Fig. 18a, the crack fracture has obvious dendritic protrusions, and it is observed that the fracture has the characteristics of a liquid column and column head. As shown in Fig. 18b, there are microcracks in the fracture, which can be judged as crystalline cracks caused by the liquid film, which can easily lead to cracking under low stress.

#### 4. Conclusions

1. Through numerical simulation, the parameters of the new test are determined finally as the number of ribs 5, the height of the rib ( $H$ ) 150 mm, the thickness of the ribs ( $T$ ) 20 mm, and the distance of the ribs ( $D$ ) 120 mm. According to the test results, the voltage has

a great influence on the crack sensitivity during the rib restraint testing method. Therefore, the welding current is determined to be 210–230 A, the arc voltage 38–40 V, and the welding speed 16–19 cm min<sup>-1</sup>.

2. The surface crack rate ( $\delta$ ) and cross-section crack rate ( $\zeta$ ) of the narrow gap test are both higher than those of the wide gap test. The reason is that the narrow gap led to a large fusion ratio, which results in the constraint stress of the rib plate being more reflected on the weld. As the restraint stress increases, the crack rate and the crack length both increase. When the crack rate is reduced to 3.6%, and the crack length is only 22 mm, it is considered critical restraint stress.

3. The method can be used to analyze the influence of various factors on crack sensitivity. The welding heat input has no significant effect on crack sensitivity when using the new test. With increasing carbon equivalent, the crack length as well as crack rate both increase.

4. Cracks that appeared in the weld center are perpendicular to the growth direction of the columnar dendrites. The aggregation of S and P was found near the crack, and the oxygen content was high. The fracture showed the characteristics of dendrites and micro-crack, which was approved as a solidification crack.

5. The new rib plate restraint method has the following three advantages: (i) By adjusting the height of the rib plate, the thickness of the rib plate, and the distance of the rib plate, the restraint stress can be adjusted very flexibly to meet the simulation of the stress state under strong restraint conditions, adapting to the application of different production conditions; (ii) The restraint design is close to the actual welding structure, more accurately reflecting the real situation of the actual welding stress and more closely matching the actual production conditions; (iii) The rib plates restraint method is more intuitive, which is conducive to reducing test costs and improving production efficiency.

### Acknowledgements

The authors would like to acknowledge the support from the National Natural Science Foundation of China (Grant No. 52105351), Postdoctoral Science Foundation of China (Grant No. 2022M722928), Natural Science Foundation of Jiangsu Province (Grant No. BK20210890), Jiangsu Provincial Double-Innovation Doctor Program (Grant No. JSSCBS20210991), and Natural Science Research Projects in Universities of Jiangsu Province (Grant No. 21KJB460015).

### References

- [1] P. Dong, F. W. Brust, Welding residual stresses and effects on fracture in pressure vessel and piping components: A millennium review and beyond, *J. Pressure Vessel Technol.* 122 (2000) 329–338. <https://doi.org/10.1115/1.556189>
- [2] C. Garza, A. Shterenlikht, M. J. Pavier, D. J. Smith, Closed-form solutions of hole distortion for use in deep-hole drilling measurements of residual stress in orthotropic plates, *J. Strain Anal. Eng. Des.* 52 (2017) 77–82. <https://doi.org/10.1177/0309324716675214>
- [3] D. A. Deng, H. Murakaw, Prediction of welding distortion and residual stress in a thin plate butt-welded joint, *Comput. Mater. Sci.* 43 (2008) 353–365. <https://doi.org/10.1016/j.commatsci.2007.12.006>
- [4] D. A. Deng, FEM prediction of welding residual stress and distortion in carbon steel considering phase transformation effects, *Mater. Des.* 30 (2009) 359–366. <https://doi.org/10.1016/j.matdes.2008.04.052>
- [5] N. Coniglio, C. E. Cross, Towards Establishment of Weldability Testing Standards for Solidification Cracking, In: T. Boellinghaus, J. Lippold, C. Cross (Eds.): *Cracking Phenomena in Welds IV*. Springer, 2016. [https://doi.org/10.1007/978-3-319-28434-7\\_3](https://doi.org/10.1007/978-3-319-28434-7_3)
- [6] S. Malarvizhi, V. Balasubramanian, Fatigue crack growth resistance of gas tungsten arc, electron beam and friction stir welded joints of AA2219 aluminium alloy, *Mater. Des.* 32 (2011) 1205–1214. <https://doi.org/10.1016/j.matdes.2010.10.019>
- [7] P. Ferro, H. Porzner, A. Tiziani, F. Bonollo, The influence of phase transformations on residual stresses induced by the welding process – 3D and 2D numerical models, *Modell. Simul. Mater. Sci. Eng.* 14 (2006) 117–136. <https://doi.org/10.1088/0965-0393/14/2/001>
- [8] H. Long, D. Gery, A. Carlier, P. G. Maropoulos, Prediction of welding distortion in butt joint of thin plates, *Mater. Des.* 30 (2009) 4126–4135. <https://doi.org/10.1016/j.matdes.2009.05.004>
- [9] M. Hirohata, Y. Itoh, High effective FE simulation methods for deformation and residual stress by butt welding of thin steel plates, *Engineering* 6 (2014) 507–515. <https://doi.org/10.4236/eng.2014.69053>
- [10] Z. B. Yang, W. Tao, L. Q. Li, Y. B. Chen, C. Y. Shi, Numerical simulation of heat transfer and fluid flow during double-sided laser beam welding of T-joints for aluminum aircraft fuselage panels, *Opt. Laser Technol.* 91 (2017) 120–129. <https://doi.org/10.1016/j.optlastec.2016.12.018>
- [11] N. S. Ma, Z. P. Cai, H. Huang, D. A. Deng, H. Murakawa, J. L. Pan, Investigation of welding residual stress in flash-butt joint of U71Mn rail steel by numerical simulation and experiment, *Mater. Des.* 88 (2015) 1296–1309. <https://doi.org/10.1016/j.matdes.2015.08.124>
- [12] E. Østby, C. Thaulow, Z. L. Zhang, Numerical simulations of specimen size and mismatch effects in ductile crack growth – Part I: Tearing resistance and crack growth paths, *Eng. Fract. Mech.* 74 (2007) 1770–1792. <https://doi.org/10.1016/j.engfracmech.2006.09.013>
- [13] G. Magudeeswaran, V. Balasubramanian, G. M. Reddy, Effect of welding processes and consumables on fatigue crack growth behaviour of armour grade

- quenched and tempered steel joints, *Def. Technol.* 10 (2014) 47–59.  
<https://doi.org/10.1016/j.dt.2014.01.005>
- [14] G. Pimenta, F. Bastian, Influence of plate thickness on the mechanical properties of welded joints subjected to long-term postweld heat treatments, *J. Mater. Eng. Perform.* 11 (2002) 130–137.  
<https://doi.org/10.1361/105994902770344187>
- [15] C. A. Correa, N. Mastelari, J. R. S. Moreno, Effect of welding parameters in flux core arc welding (FCAW) with conventional and pulsed current in the efficiency and fusion rate of melting coating, *Sci. Res. Essays* 9 (2014) 976–983.  
<https://doi.org/10.5897/SRE2014.6064>
- [16] M. R. Nezamdost, M. R. N. Esfahani, S. H. Hashemi, S. A. Mirbozorgi, Investigation of temperature and residual stresses field of submerged arc welding by finite element method and experiments, *Int. J. Adv. Des. Manuf. Technol.* 87 (2016) 615–624.  
<https://doi.org/10.1007/s00170-016-8509-4>
- [17] G. A. Bilenko, Use of the program SYSWELD to analyze residual stresses and strains after the welding of pressure vessels, *Metallurgist* 56 (2012) 565–569.  
<https://doi.org/10.1007/s11015-012-9616-6>